Reversible Phase Transition of Colloids in a Binary Liquid Solvent

Hua Guo,[1] Theyencheri Narayanan,[2] Michael Sztuchi,[2] Peter Schall,[1] and Gerard H. Wegdam[1]

[1]*Van der Waals-Zeeman Institute, University of Amsterdam, 1018XE Amsterdam, The Netherlands*

[2]*European Synchrotron Radiation Facility, F-38043, Grenoble, France*

(Received 12 December 2007; published 6 May 2008)

We report fluid-fluid and fluid-solid phase transitions of charge-stabilized polystyrene particles suspended in a binary liquid mixture of 3-methylpyridine and water. These thermally reversible phase transitions occur in the homogeneous phase of the binary liquid mixture below the coexistence temperature of the two liquids. Close density matching of the particles and the solvent allows us to follow the phase behavior until complete coexistence of macroscopic phases with temperature as the control parameter. We use small angle x-ray scattering to characterize these phases as colloidal gas, liquid, fcc crystal, and glass.

DOI: 10.1103/PhysRevLett.100.188303 PACS numbers: 82.70.Dd

Colloidal systems with an attractive interparticle potential exhibit a rich phase behavior with solid, liquid, and gas phases [1,2]. The commonly used method to introduce an attractive interaction is by the addition of nonadsorbing polymers to an otherwise repulsive colloidal suspension [2]. The control parameters for this depletion attraction are the size and concentration of the added polymers. Even in charge-stabilized colloidal systems without polymers, attractive forces often arise under certain special conditions [3]. For instance, at interfaces and in confined geometries, condensation into ordered structures with open voids and metastable clusters were found. Crocker and Grier reported a direct measurement of an attractive potential close to an interface [4]. Not only at interfaces but also in bulk systems, an attractive interaction has to be invoked to account for the observed phenomena such as vapor-liquid condensation [5], amorphous structures [6], and long-lived metastable crystallites [5]. In biological systems, the short-range attraction plays a crucial role in their self-assembly and protein crystallization [7].

Attractive interactions also arise when charge-stabilized colloidal particles are suspended in binary liquid solvents. Beysens and Esteve observed a reversible aggregation of silica particles in a binary mixture of 2,6-lutidine and water by approaching the bulk phase coexistence temperature (T_{cx}) of the mixture [8]. Charge-stabilized colloidal particles in binary mixtures have a unique feature that sets them aside from other systems. Temperature can be used as an external parameter to control the amplitude and range of the attractive force. Anomalies in surface energy near T_{cx} lead to a temperature-dependent adsorption onto the colloidal particles which controls the colloidal interaction [9]. Thus temperature offers a convenient means to study the phase behavior of the colloidal system with external control. Similar phase behavior is also observed in different types of binary mixtures and colloidal particles [9–11].

In this Letter, we show that the ''aggregation'' observed by Beysens and Esteve is a reversible phase transition for the colloidal system. Density matching between the particles and the suspending medium enabled us to observe stable gas-liquid and gas-solid equilibria. In a density-matched system the nuclei can, in principle, grow to macroscopic dimensions, while in a nondensity-matched system gravity perturbs this growth process at a very early stage. The phases are characterized by synchrotron small angle x-ray scattering (SAXS). The observation of gas-liquid and gas-solid phase transitions in this system is consistent with an effective attractive potential of mean force approach used in earlier studies [10,12]. The gas-liquid equilibrium that we observe suggests the existence of a long-range attraction in this system.

The experimental system consists of charge-stabilized polystyrene spheres suspended in a mixture of 3-methylpyridine (3MP), water, and heavy water with weight fractions of $C_{3MP} = 0.25$, $C_{H_2O} = 0.5625$, and $C_{D_2O} = 0.1875$, respectively. For this liquid mixture without the colloids, T_{cx} is around 65 °C [13]. The water-to-heavy water ratio is chosen such that the density of the liquid mixture closely matches that of the particles in the temperature region where the transition occurs. The particles have a diameter of 105 nm with a polydispersity of 3.5% determined from the scattering form factor and an effective surface charge density of $-0.4\ \mu C/cm^2$, measured in the binary mixture by electrophoresis at room temperature. The 3MP and heavy water were purchased from Aldrich chemicals, and the water was deionized Millipore water (MilliQ). The dielectric constant of 3MP at room temperature at the visible wavelength range is about 9.8. Six samples were made with particle volume fractions of $\phi = 0.0025$, 0.005, 0.010, 0.015, and 0.05 and a reference sample without colloidal particles. The samples were contained in flat borosilicate capillaries with an optical path length of 1.0 mm, which were flame-sealed to avoid solvent evaporation. The glass surfaces were thoroughly cleaned with chromic acid and rinsed with Millipore water to guarantee a clean OH surface and to avoid contaminations that might influence the phase behavior. The samples were studied by SAXS at the beam line ID02 of the European Synchrotron facility (ESRF). Samples were placed in a thermostatted oven with a temperature stability

better than 2 mK [12]. We raised the temperature in steps of 0.05 K, waited for 5 min after each temperature increment to let the system equilibrate, and recorded the scattered intensity. This corresponds to an average heating rate of 10^{-4} K/s. The measured two-dimensional SAXS patterns were normalized and azimuthally averaged to obtain the intensity $I(q)$ as a function of the scattering vector $q = (4\pi/\lambda)\sin(\theta/2)$, with θ the scattering angle and $\lambda = 1$ Å the wavelength of incident x rays. Transition temperatures were also verified by measurement of the sample turbidity. For direct visual observation, the samples were placed in a thermostatted water bath, and direct images of the samples were taken with a CCD camera.

Figure 1(a) depicts the schematic phase diagram of the quasibinary solvent mixture (one phase at temperatures below T_{cx} and two phases at temperatures above T_{cx}) and the region in which the colloidal particles aggregate [9]. This aggregation occurs at a sharply defined aggregation temperature T_a. We start with a homogenous suspension at room temperature (sample 1). When the temperature approaches $T_a = 330.5$ K, we observe that the system separates into a colloid-rich and a colloid-poor phase as shown by regions of high and low turbidity (sample 2). When crossing the phase separation temperature T_{cx}, the binary liquid solvent separates into 3MP-rich and 3MP-poor phases, as indicated by the occurrence of a sharp liquid-liquid interface, and we observe that the particles assemble in the 3MP-rich phase (sample 3). In the following, we focus on regions (1) and (2) and use SAXS to characterize the colloidal phases formed.

Figure 2 presents the evolution of SAXS intensity for the sample of volume fraction 0.05, as the temperature was raised from 300 to 332.5 K. At $T = 330.3$ K, the intensity profile (curve I) is similar to that of the form factor, which was determined from a very dilute sample with volume fraction 0.0005. After subtraction of the background scattering due to the suspending fluid and division by the form factor, we obtained the corresponding structure factor depicted in Fig. 2(b)(I). The structure factor is essentially 1 over the whole wave vector range. When the temperature was raised by 0.2 K, we observed the appearance of a pronounced peak (curve II) as shown by the structure factor in Fig. 2(b)(II). This structure factor is typical for a liquid or a dense fluid phase. With increasing temperature, the height of the peak increased continuously until $T = 332.50$ K (curve III), where it suddenly jumped to a value above 2.85, the freezing criterion [14]. We also observed that the peak narrows and higher order reflections appear: The liquid has turned into a solid. When we lowered the temperature back to 330.30 K, we obtained spectrum IV, which is indistinguishable from I: The solid melts, and the suspension is back in the gas phase. This whole process can be repeated several times. The transition is reversible, and we do not see any appreciable hysteresis.

The peaks in the structure factor of the solid phase in Fig. 2(b) are located at q values in the ratio $\sqrt{3}:\sqrt{4}:\sqrt{8}:\sqrt{11}:\sqrt{12}$. These peak positions are characteristic of the face-centered cubic (fcc) lattice [15]. The

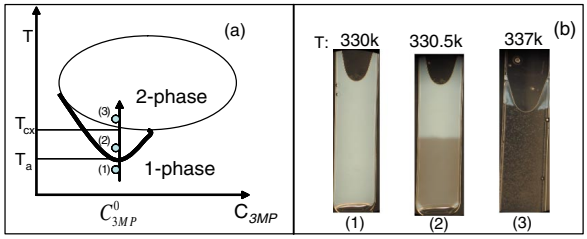

FIG. 1 (color online). (a) Schematic state diagram of polystyrene particles in a quasibinary mixture of 3MP/H_2O/D_2O. The numbers label characteristic regimes, the corresponding states of which are illustrated in (b). In regime (2), the aggregation of colloids takes place. (b) Photographs of sample cells illustrating the macroscopic state of the dispersion in regions (1)–(3) of the phase diagram.

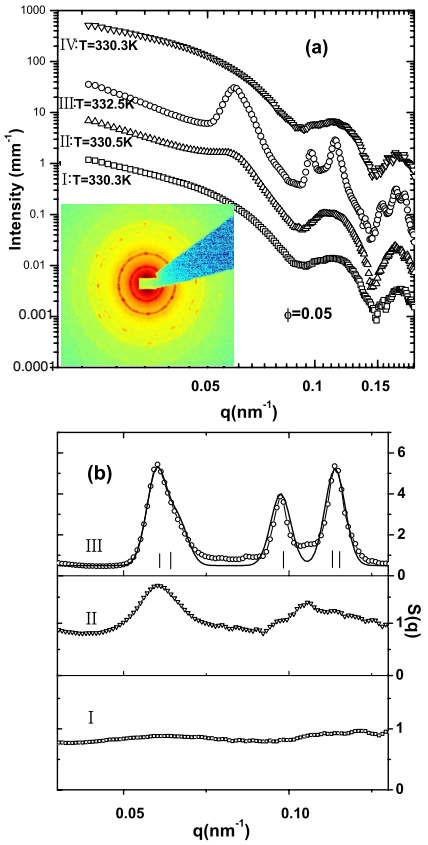

FIG. 2 (color online). (a) SAXS intensity profiles in the vicinity of T_a. Curves I–IV correspond to temperatures of 330.3, 330.5, 332.5, and 330.3 K, respectively. Successive curves have been displaced along the intensity axis by a factor of 10 for the sake of clarity. The inset shows the 2D scattering pattern corresponding to curve III. (b) Structure factors corresponding to the intensity profiles $I(q)$ in (a). These demonstrate the transition from gas (I) to liquid (II) and solid (III). The ticks at the bottom in (III) indicate the peak positions for an fcc crystal with lattice constant $d = 181$ nm. The solid line indicates the structure factor calculated for fcc crystals of average size ~900 nm.

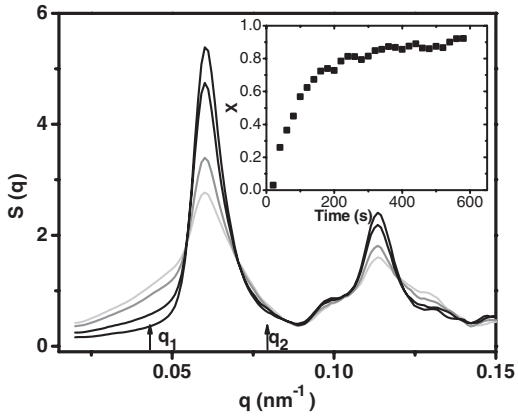

FIG. 3. Time evolution of the structure factor $S(q)$ at constant temperature during crystal growth from the gas phase. The window used in the calculation of the moments of the peak is indicated by $q1$ and $q2$. The time evolution of the crystallinity $X(t)$ is shown in the inset.

observed peaks correspond to (111), (200), (220), (311), and (222), respectively. From the absolute values of q indicated by ticks in Fig. 2(b)(III), we calculated the cubic crystal lattice constant to be 181 nm. By using this lattice parameter and the radius of the particles determined from the form factor $R = 52.5$ nm, we determined the volume fraction of particles $\phi_{\mathrm{fcc}} = 0.406$. The peaks in Fig. 2(b)(III) can be fitted with Gaussian functions with a full width at half maximum of $\Delta q = 0.007$ nm^{-1}, which is significantly larger than the instrument resolution ≈ 0.003 nm^{-1}. The fitted width corresponds to an average crystallite size of $l_c \approx 2\pi/\Delta_q \approx 900$ nm. The hexagonal symmetry of the diffraction peaks in the two-dimensional SAXS pattern [see Fig. 2(a), inset] indicates that the fcc crystals are preferentially oriented with their hexagonal close-packed planes parallel to the glass wall of the capillary [15].

For the samples with volume fractions ≤ 0.015, we did not observe the liquid phase. The solid formed directly from the low density fluid. We noticed a sudden transition from a flat structure factor to that of the fcc crystal. We followed the crystal growth process as a function of time by keeping the temperature constant as soon as the crystal peaks appear and recording diffraction patterns every 30 seconds. We show the time evolution of the crystalline structure factor from the sample with $\phi = 0.01$ in Fig. 3. The peaks grow in height, while the width and the position remain nearly the same. This means that the size of the crystallites remains constant within the instrument resolution, and their number density increases with time. The area under the main peak

$$X(t) = c \int_{q1}^{q2} S(q, t) dq, \qquad (1)$$

where c is a normalization factor and the integration limits are indicated in Fig. 3, is proportional to the amount of colloids in the scattering volume that has been converted to a solid phase, and we define this to be a measure of the crystallinity [16]. The time dependence of $X(t)$ is illustrated in the inset in Fig. 3 showing a saturation of X at times larger than about 200 s. The crystallization occurs at a constant number of particles, and with time more particles are accommodated in crystalline lattices as indicated by the decreasing intensity at low q. The width of the Bragg peaks may be limited by the finite instrument resolution and significant local oscillations of the particles in the crystal lattice.

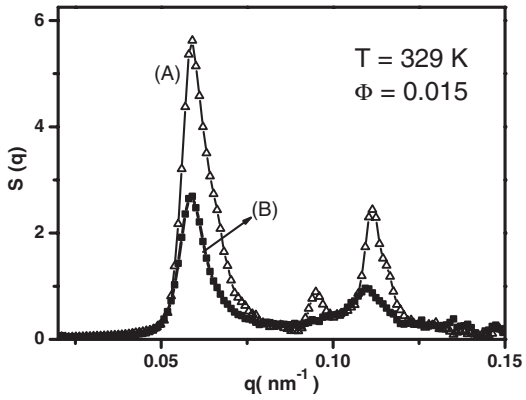

FIG. 4. Dependence of the structure on the heating rate. Structure factors $S(q)$ measured at $T = 329$ K after heating at a rate of (B) 10^{-3} and (A) 10^{-4} K/s.

We have shown that we can induce reversible solidification and melting in our colloidal system by just changing the temperature. This temperature control allows us to study kinetic effects in the formation of these phases by choosing different heating rates. We repeated the experiment and chose a temperature increase in steps of 0.5 instead of 0.05 K, which corresponds to an average heating rate of 10^{-3} instead of 10^{-4} K/s. The structure factors of the samples obtained with both heating rates and measured at the same temperature are presented in Fig. 4. To our surprise we found structure factor (B) at the higher heating rate, which does not show the characteristic crystal peaks

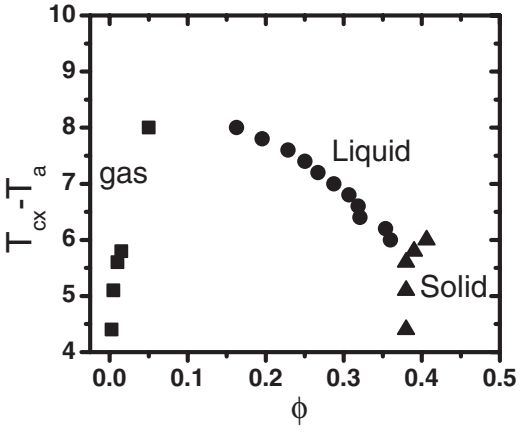

FIG. 5. Phase diagram of polystyrene spheres in the quasibinary mixture 3MP/H_2O/D_2O. Triangles, solid circles, and squares mark the temperatures $\Delta T = T_{cx} - T_a$ versus volume fraction ϕ for solid, liquid, and gas phases, respectively.

but shows the signature of a glass: The height of the first peak is 2.6, and the higher order reflections are less pronounced except the second peak. Both structure factors remained constant in time when we stopped the temperature rise. We conclude that, at this higher heating rate, we ''quenched'' the system into a glassy state, analogous to glass formation in a molecular system.

The phase behavior that we observe with SAXS, turbidity measurement, and visual observation is summarized in a phase diagram for the colloidal system in Fig. 5, where we plot $\Delta T = T_{cx} - T_a$ versus the volume fraction. From all of the data obtained for colloids in binary liquid mixtures, it is clear that this temperature difference is the experimentally relevant parameter to describe the state of the colloidal system. At low volume fractions, the colloidal system shows two stable phases: fluid and crystal. At higher volume fractions, we observe equilibria of gas and liquid and liquid and solid. The volume fraction of particles in the gas phase is set to the initial volume fractions of the samples that we prepared. The volume fraction in the solid phase is determined from the crystal lattice constant and particle radius as described above. For the volume fraction of the liquid, we fit the structure factor to an effective hard-sphere model. As a reference state we take the liquid in equilibrium with the solid under the assumption that the liquid-solid gap is the same as that of hard spheres. With this reasonable assumption, we came to the volume fraction of liquid and indicated them by solid circles in Fig. 5. The similarity of the diagram presented in Fig. 5 with the diagrams suggested by Frenkel [1] for attractive colloidal systems is striking. The existence of a gas-liquid coexistence region before the liquid-solid coexistence suggests that there is a long-range attractive potential.

What is the origin of this attractive potential? Fisher and de Gennes [17] suggested that the preferential or preferred adsorption of one of the liquids onto the surface of the colloidal particles leads to a reduction of the free energy when the adsorption layers of adjacent particles overlap. The range of attraction is then determined by the thickness of the adsorption layer which is of the order of the bulk correlation length of the binary solvent. In our system, it is about 8 nm at $T = T_a$ as determined from static light scattering. This value is smaller than the distance of 25 nm between the particle surfaces in the solid phase, calculated from their nearest neighbor distance, and larger than the Debye screening length of 6.5 nm, estimated from the effective radius [18]. Recent density functional theory indeed predicts a bridging transition as two particles with adsorbed layers approach each other and the resulting effective potential becomes long ranged and strongly attractive [19].

Law, Petit, and Beysens calculated the Derjaguin-Landau-Verweg-Overbeek potential involving the screened Coulomb repulsion and the van der Waals attraction for the case of particles with an adsorbed layer [20]. They found that the adsorption layer reduces dramatically the stabilizing repulsive barrier due to the different Debye screening length within the adsorption layer as compared to the bulk. They estimated that, in a dilute suspension of silica in 2,6-lutidine and water, an adsorbed layer thickness of about 12 nm is sufficient to destabilize the suspension and induce particle aggregation. The absorption layer thickness of about 8 nm that we estimated is in agreement with this scenario. More recent numerical simulations proposed a wetting-induced dynamic depletion force that can be much stronger than the van der Waals attraction and consequently lead to particle aggregation [21]. All of these mechanisms could play a role at different stages of phase transitions that we reported here.

In summary, we have observed the formation of solid and liquid colloidal phases in equilibrium with a dilute gas phase with only the temperature as a control parameter. Our system allows further investigation of the rich phase behavior of attractive colloidal systems by using temperature as an external control parameter.

The research has been supported by the Foundation for Fundamental Research on Matter (FOM), which is financially supported by Netherlands Organization for Scientific Research (NWO). We thank ESRF for the beam time.

[1] D. Frenkel, Science **314**, 768 (2006).
[2] V. J. Anderson and H. N. W. Lekkerkerker, Nature (London) **416**, 811 (2002).
[3] L. Belloni, J. Phys. Condens. Matter **12**, R549 (2000).
[4] J. C. Crocker and D. G. Grier, Phys. Rev. Lett. **73**, 352 (1994).
[5] A. K. Arora and B. V. R. Tata, Adv. Colloid Interface Sci. **78**, 49 (1998).
[6] E. B. Sirota and P. M. Chaikin, Phys. Rev. Lett. **62**, 1524 (1989).
[7] A. Tardieu *et al.*, J. Cryst. Growth **196**, 193 (1999).
[8] D. Beysens and D. Esteve, Phys. Rev. Lett. **54**, 2123 (1985).
[9] D. Beysens and T. Narayanan, J. Stat. Phys. **95**, 997 (1999).
[10] S. R. Kline and E. W. Kaler, Langmuir **10**, 412 (1994).
[11] Y. Jayalakshmi and E. W. Kaler, Phys. Rev. Lett. **78**, 1379 (1997).
[12] D. Pontoni, T. Narayanan, J.-M. Petit, G. Grubel, and D. Beysens, Phys. Rev. Lett. **90**, 188301 (2003).
[13] T. Narayanan and A. Kumar, Phys. Rep. **249**, 135 (1994).
[14] H. Lowen, Phys. Rep. **237**, 249 (1994).
[15] W. L. Vos, M. Megens, C. M. van Kats, and P. Boesecke, Langmuir **13**, 6004 (1997).
[16] H. J. Schope, G. Bryant, and W. van Megen, J. Chem. Phys. **127**, 084505 (2007).
[17] M. E. Fisher and P. G. de Gennes, C.R. Acad. Sci. Ser. B **287**, 207 (1978).
[18] R. J. Hunter, *Foundations of Colloid Science* (Clarendon Press, Oxford, 1992), Vol. II.
[19] A. J. Archer, R. Evans, R. Roth, and M. Oettel, J. Chem. Phys. **122**, 084513 (2005).
[20] B. M. Law, J.-M. Petit, and D. Beysens, Phys. Rev. E **57**, 5782 (1998).
[21] T. Araki and H. Tanaka, J. Phys. Condens. Matter **20**, 072101 (2008).